Petroleum Science 19 (2022) 720–730

Contents lists available at ScienceDirect

Petroleum Science

journal homepage: www.keaipublishing.com/en/journals/petroleum-science

Original Paper

Research on properties of hollow glass microspheres/epoxy resin composites applied in deep rock in-situ temperature-preserved coring

Zhi-Qiang He [a, b, c], Yang Yang [a, *], Bo Yu [d], Jian-Ping Yang [e], Xiang-Biao Jiang [f], Bo Tian [g], Man Wang [h], Xi-Yuan Li [h], Si-Qing Sun [i], Hui Sun [i]

[a] State Key Laboratory of Hydraulics and Mountain River Engineering, MOE Key Laboratory of Deep Earth Science and Engineering, College of Water Resource and Hydropower, Sichuan University, Chengdu 610065, Sichuan, China
[b] Guangdong Provincial Key Laboratory of Deep Earth Sciences and Geothermal Energy Exploitation and Utilization, Institute of Deep Earth Sciences and Green Energy, College of Civil and Transportation Engineering, Shenzhen University, Shenzhen 518060, Guangdong, China
[c] Shenzhen Key Laboratory of Deep Underground Engineering Sciences and Green Energy, Shenzhen University, Shenzhen 518060, Guangdong, China
[d] School of Mechanical Engineering, Sichuan University, Chengdu 610065, Sichuan, China
[e] College of Polymer Science and Engineering, Sichuan University, Chengdu 610065, Sichuan, China
[f] Changsha High tech Automation Equipment Co., LTD Changsha 410100, Hunan, China
[g] Jinshi Drilltech co., Ltd, Tangshan 063000, Hebei, China
[h] State Key Laboratory of Coking Coal Exploitation and Comprehensive Utilization, Institute of Coal Mining and Utilization, Pingdingshan Tianan Coal Mining Co., LTD., Pingdingshan 467000, China
[i] Xi'an Research Institute, China Coal Technology & Engineering Group Corp, Xi'an 710077, China

ARTICLE INFO

Article history:
Received 2 July 2021
Accepted 28 October 2021
Available online 1 November 2021

Edited by Yan-Hua Sun

Keywords:
Deep rock in-situ temperature-preserved coring (ITP-Coring)
Hollow glass microspheres/epoxy resin composites
Hydrostatic pressure
Unsteady-state heat transfer model

ABSTRACT

Deep petroleum resources are in a high-temperature environment. However, the traditional deep rock coring method has no temperature preserved measures and ignores the effect of temperature on rock porosity and permeability, which will lead to the distortion of the petroleum resources reserves assessment. Therefore, the hollow glass microspheres/epoxy resin (HGM/EP) composites were innovatively proposed as temperature preserved materials for in-situ temperature-preserved coring (ITP-Coring), and the physical, mechanical, and temperature preserved properties were evaluated. The results indicated that: As the HGM content increased, the density and mechanical properties of the composites gradually decreased, while the water absorption was deficient without hydrostatic pressure. For composites with 50 vol% HGM, when the hydrostatic pressure reached 60 MPa, the water absorption was above 30.19%, and the physical and mechanical properties of composites were weakened. When the hydrostatic pressure was lower than 40 MPa, the mechanical properties and thermal conductivity of composites were almost unchanged. Therefore, the composites with 50 vol% HGM can be used for ITP-Coring operations in deep environments with the highest hydrostatic pressure of 40 MPa. Finally, to further understand the temperature preserved performance of composites in practical applications, the temperature preserved properties were measured. An unsteady-state heat transfer model was established based on the test results, then the theoretical change of the core temperature during the coring process was obtained. The above tests results can provide a research basis for deep rock in-situ temperature preserved corer and support accurate assessment of deep petroleum reserves.

1. Introduction

The shallow mineral resources have been gradually exhausted, and attention have been paid to mineral exploitation in deep earth (Xie et al., 2015; Zhang et al., 2016; Gao et al., 2020b, 2021b). For example, current petroleum resources exploitation has reached 7500 m. Therefore, deep mining is an ongoing mining industry (Gao et al., 2018; Gao et al., 2020a). Deep petroleum resources universally are in a high temperature environment (Pang et al., 2015), and the influence of temperature will cause great changes in rock permeability and seepage laws (Liang et al., 2005). Saif et al.

* Corresponding author.
E-mail address: yangyang6463@126.com (Y. Yang).

https://doi.org/10.1016/j.petsci.2021.10.028

(2017) obtained that connected pores and cracks appeared in oil shale under high temperature through microtomography. Rabbani et al. (2017) found that permeability is related to the connectivity of pores and cracks. Zhao et al. (2012) found that the porosity of oil shale samples from Daqing and Yan'an cities increased significantly in the range of 100–200 °C. The evaluation and exploitation of underground petroleum resources are closely related to the porosity and permeability of reservoir, which affect the accurate evaluation of petroleum resources (Zhou et al., 2010). Scientific drilling is an important mean in the field of petroleum resources exploration. However, due to the inability to temperature-preserved coring for continental deep rock, the distortion of core temperature will result in the incomplete scientific acquisition of resources reserves and gas phase information. Therefore, it is necessary to develop ITP-Coring equipment to preserve the in-situ temperature of the core occurrence environment, and provide a basis for subsequent tests (Xie et al., 2020; He et al., 2020; Gao et al., 2021a).

The focus of deep continental coring is still on the drilling technology. Only deep-sea corers have taken the lead in coring technology with retaining in-situ conditions of sediments (Rothwell and Rack, 2006). However, these devices are mainly designed for retaining pressure, and most of them do not consider temperature preserved. Instead, the corer is placed in a cooler when the devices is lifted, such as the Multiple Autoclave Corer (MAC) and the Dynamic Autoclave Piston Corer (DAPC) (Abegg et al., 2008). Only a few deep-sea corers involve temperature preserved technology. Pressure Temperature Core Sampler (PTCS) and High-Pressure-Temperature-Corer (HPTC) adopt double-layer inner pipe for temperature preservation (Norihito and Koji, 2015; Takahashi and Tsuji, 2005; Zhu et al., 2011). Zhu et al. (2013) developed a Pressure and Temperature Preservation System (PTPS), which adopted a double-layer temperature preserved structure with an inner surface sprayed with temperature preserved material, an outer surface sprayed with an anti-ultraviolet coating and combined with a vacuum in the interlayer. The fidelity coring device developed by Zhejiang University adopted temperature preserved coating and double-layer pipe (Li et al., 2006; Qin et al., 2005). However, the temperature preserved materials of the above-mentioned corers are all implemented by sandwiching, which increases the corer wall thickness and diameter of the core hole, increasing in the cost of coring. Meanwhile, deep rocks are in an environment with high hydrostatic pressure, and ordinary temperature preserved materials that do not use sandwich structure will not be suitable for deep rock ITP-Coring.

HGM/EP composites have the advantages of low water absorption, high strength and low thermal conductivity (Yung et al., 2009). They are widely used as solid buoyancy materials in deep-sea and pipeline temperature preserved materials for deep-sea oil, etc. (Gupta et al., 2014). Many scholars have carried out related research on HGM/EP composites. Gupta et al. (2001) summarized the form of the compressive stress-strain curve of composites with a different aspect ratios of specimens. Kim and Plubrai (2004) analyzed two failure modes of composites with different HGM volume fractions. Gall et al. (2014) and Ozturk and Anlas (2011) tested the volumetric strain of composites in hydrostatic pressure. Zhai et al. (2020) used a rock mechanics testing system to characterize the mechanical properties of composites. Xing et al. (2020) established a three-phase thermal conductivity model to predict the thermal conductivity of composites, which is in good agreement with the test results. Wang (2017) derived a heat transfer model for deep-sea oil pipelines based on composites for temperature preservation.

Based on the concept of deep rock ITP-Coring proposed by Xie et al. (2020, 2021), in order to eliminate the sandwich structure while taking into account the deep environmental characteristics of high hydrostatic pressure and high temperature (Gao et al., 2021c; Xie, 2017), HGM/EP composites are proposed as the temperature preserved materials for deep rock ITP-Coring. However, few scholars have studied the properties of composites after hydrostatic pressure treatment. Therefore, the physical, mechanical, and temperature preserved properties of composites with different content of K1-HGM (hollow glass microspheres of K1 type) were tested. Meanwhile, considering the coring environment of high hydrostatic pressure, the above properties of 50 vol% K1-HGM/EP composites were also studied. Finally, an unsteady-state heat transfer model based on composites was established, and the theoretical change law of the core temperature during the coring process was obtained.

2. The properties of composites with different content of HGM

2.1. Sample preparation of HGM/EP composites

The composites are prepared using E51 epoxy resin as the substrate (1.15 g/cm^3), 2-ethyl-4-methylimidazole as the curing agent, and K1-HGM from 3M Scotchlite™ as the filler. The proportion of curing agents is 5%. The HGM is added to the epoxy resin several times in small quantities, and mixture is evenly stirred at a speed of 50 r/min before pouring into the mould. The curing process of the composites is 80 °C/1 h + 170 °C/3 h. The parameters of K1-HGM are shown in Table 1. To explore the composites suitable for ITP-Coring, composites with different content of K1-HGM (0, 10 vol%, 20 vol%, 30 vol%, 40 vol%, and 50 vol%) are prepared.

2.2. Density and water absorption of composites with different HGM content

Fig. 1 shows the density of composites with different HGM content. Since the density of HGM is much lower than that of epoxy resin, and the addition of HGM will also introduce bubbles to form pores. Then, the density of composites shows a significant downward trend as the K1-HGM content increases. As the K1-HGM content increases from 0 to 50 vol%, the density decreases from 1.18 g/cm^3 to 0.7 g/cm^3, showing a good linear relationship overall.

The deep environment is rich in pore water, and the properties of composites will change after absorbing water, so the water absorption of the composites needs to be researched. Considering that the coring process is about 2 h, the prepared samples are placed in water without pressure for 2 h, and the water absorption is obtained by measuring the mass before and after the test (as shown in Fig. 2). Due to the measurement error, the water absorption of composites with different K1-HGM content fluctuates slightly, but the water absorption rate is shallow overall. The composites have good waterproof performance, and composites are feasible to be applied in ITP-Coring.

2.3. Thermal conductivity and thermal diffusivity of composites with different HGM content

Thermal conductivity and thermal diffusivity are important parameters to measure the temperature preserved performance of materials. The test instrument was the Hot Disk Thermal Constant Analyzer TPS2500 S.

Fig. 3 shows the thermal conductivity and thermal diffusivity of composites with different HGM content. Due to the addition of HGM, the density of the material is significantly reduced (as shown in Fig. 1), which leads to a sharp increase in the porosity of the composites. The inside of HGM is a vacuum or a rare gas, and its

Table 1
The parameters of K1-HGM.

Hollow glass microspheres type	Typical density, g/cm^3	Particle size distribution, mm			Isostatic crush strength, MPa
		D_{10}	D_{50}	D_{90}	
K1	0.125	30	65	110	1.72

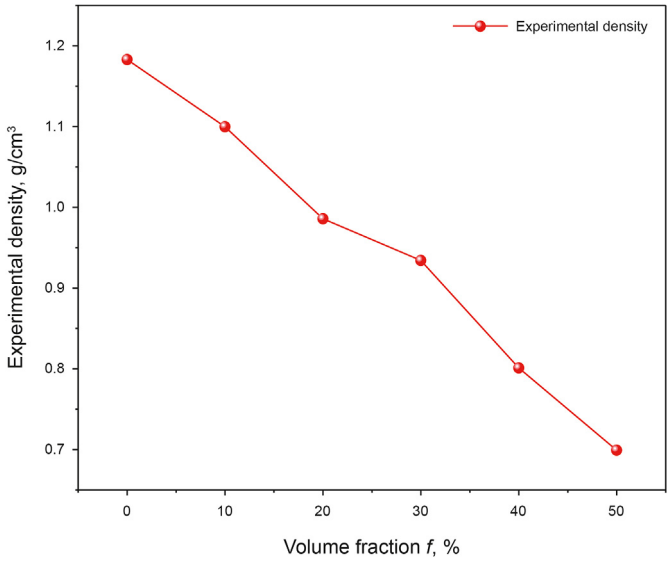

Fig. 1. The density of composites with different HGM content.

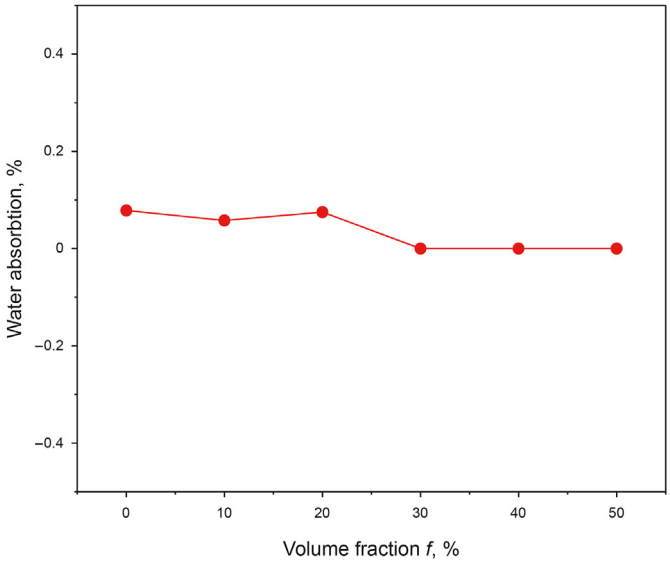

Fig. 2. The water absorption of composites with different HGM content.

thermal conductivity is extremely low. Therefore, the thermal conductivity decreases sharply after forming the composites with epoxy resin. Fig. 4 shows that when the content is less than 30 vol%, the mixing of HGM is not uniform, so the thermal conductivity and thermal diffusivity of the composites are not significantly reduced. When the content reaches 40–50 vol%, the uniformly mixed HGM reduce the thermal conductivity to 0.148 W/(m·K). Moreover, Fig. 5 shows the SEM images of composites with different HGM content.

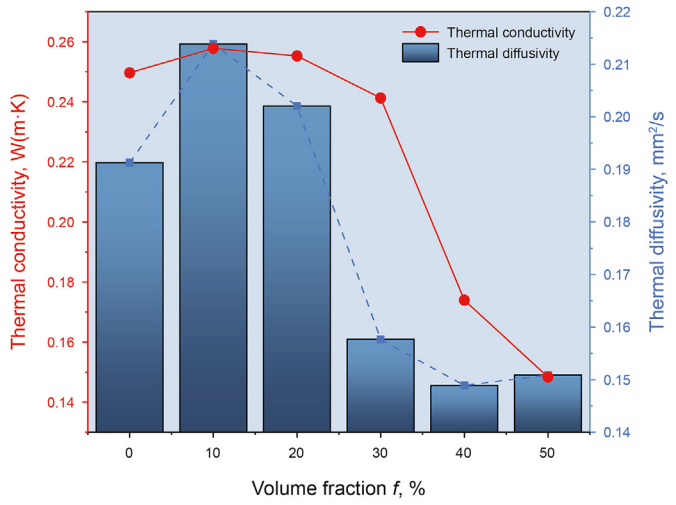

Fig. 3. Thermal conductivity and thermal diffusivity of composites with different HGM content.

2.4. Mechanical properties of composites with different HGM content

The coring environment requires that the composites meet the coordinated deformation of the corer (strain reaches 0.25%) and has sufficient strength to prevent the loss of temperature preserved ability due to falling off and cracking. Therefore, the compression and tensile tests of composites with different HGM content are conducted to evaluate the mechanical properties of the composites. The test instrument is the Instron Universal Material Testing Machine.

Fig. 6 shows the ultimate compressive and tensile strengths of composites with different HGM content. Since the strength of K1-HGM is much lower than that of epoxy resin, as the HGM content increases, the epoxy resin substrate between the HGM becomes thinner, and the compressive and tensile strengths of the composites gradually decrease. The compressive and tensile strengths are 45.53 MPa and 13.25 MPa, respectively when the content increases to 50 vol%, which are 66.92% and 70.46% lower than the materials without the addition of HGM. Fig. 7 shows the ultimate compressive and tensile strains of composites with different HGM content. The strains also decrease significantly with the increase in HGM content. Overall, the addition of HGM has weakened the composites. When the content is 50 vol%, the compressive and tensile strains are 7.04% and 0.90%, respectively, which meet the strain requirements required for application in the corer.

3. The change of properties of composites after hydrostatic pressure treatment

Since deep rocks exist in high hydrostatic pressure environments, whether composites can be applied requires further exploration of the composites with 50 vol% HGM has the lowest thermal conductivity and meets the strain and strength

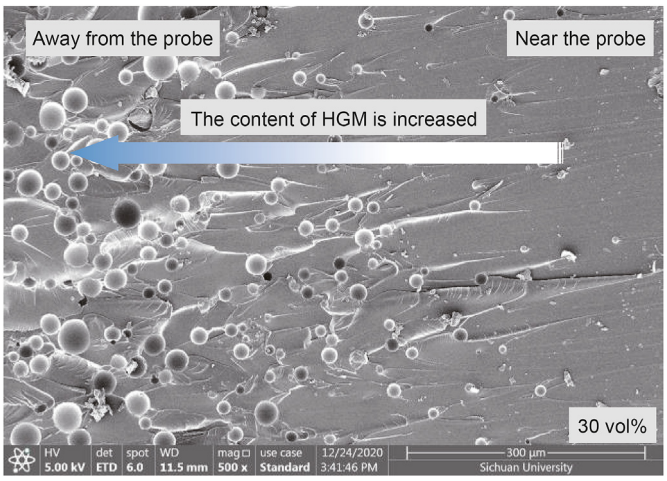

Fig. 4. Distribution of HGM in composites.

requirements. Therefore, composites with 50 vol% HGM were treated by high hydrostatic pressure (10, 20, 40, 60 MPa), then the influence mechanism of hydrostatic pressure on properties of composites were investigated.

3.1. The water absorption change of composites after hydrostatic pressure treatment

The water absorption of composites with 50 vol% HGM after different hydrostatic pressure treatments are shown in Fig. 8. The water absorption of the composites fluctuates slightly when the hydrostatic pressure is lower than 40 MPa, but it does not exceed 2%. When the pressure reaches 60 MPa, the water absorption rises sharply, and the water absorption of specimens for compression, thermal conductivity and tensile tests reach 49.65%, 50.39%, and 30.19%, respectively. The cured epoxy resin will form a dense network structure also bond with HGM to form the composites. With an increase in the hydrostatic pressure, water invades the interface layer of HGM and the epoxy resin matrix and the pores, this may cause damage to the HGM (as shown in Fig. 9). The reason for the difference in water absorption of various types of samples may be caused by factors such as different specifications and sizes of the samples. For example, the theoretical specific surface areas of the compression, tension and thermal conductivity are 0.7, 0.4, 0.001 m^2/kg, indicating that the larger the specific surface area, the higher the water absorption. According to the test results, the critical hydrostatic pressure of the composites with 50 vol% HGM is

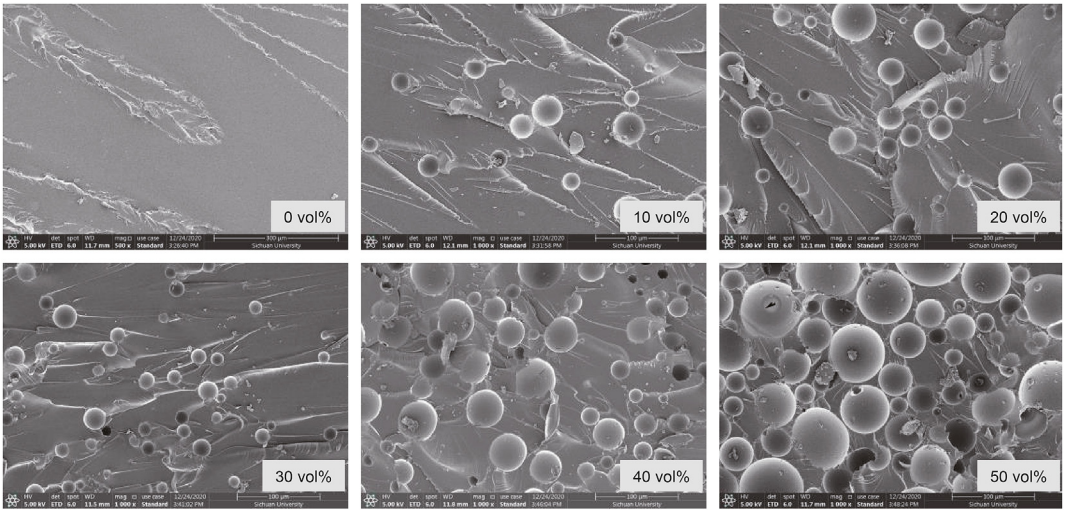

Fig. 5. The SEM images of composites with different HGM content.

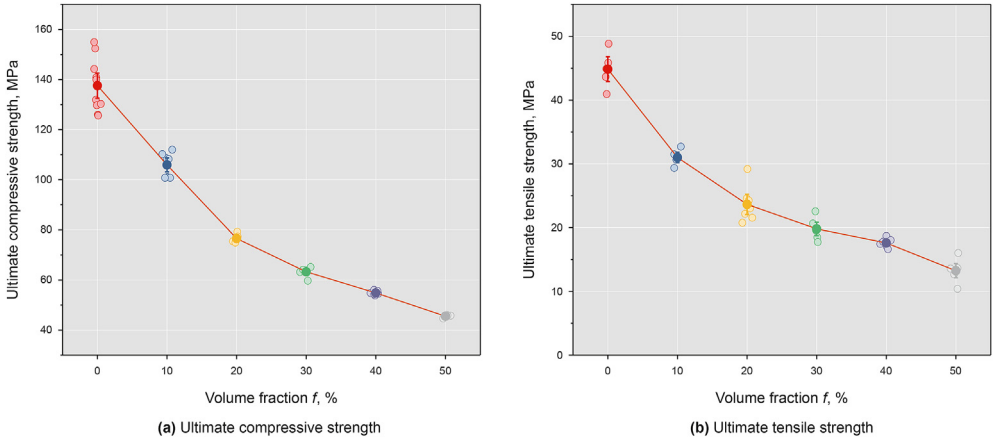

Fig. 6. Ultimate compressive and tensile strengths of composites with different HGM content.

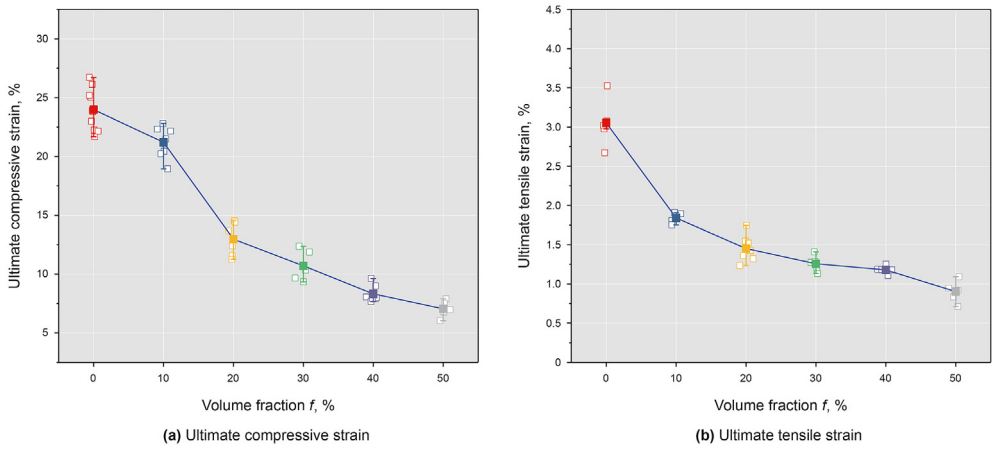

Fig. 7. Ultimate compressive and tensile strains of composites with different HGM content.

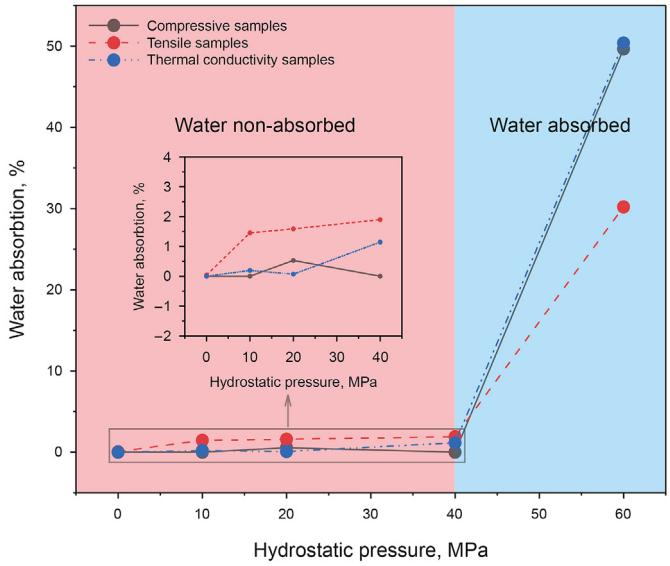

Fig. 8. The water absorption of composites with 50 vol% HGM after different hydrostatic pressure treatments.

about 40 MPa, which means that it can be applied to ITP-Coring with a hydrostatic pressure of up to 40 MPa.

3.2. The thermal conductivity and thermal diffusivity change of composites after hydrostatic pressure treatment

Fig. 10 shows the thermal conductivity and thermal diffusivity of composites after different hydrostatic pressure treatments. The change of thermal conductivity and thermal diffusivity conforms to the trend of water absorption. When the hydrostatic pressure reaches 60 MPa, the thermal conductivity and thermal diffusivity of the composites increase sharply, and the thermal conductivity reaches 0.3474 W/(m·K), which increases by about 2.34 times. However, when the hydrostatic pressure is less than 40 MPa, the thermal conductivity of the composites hardly changes because it does not absorb water.

The mechanism of temperature preserved materials is blocking the heat transfer and slowing the heat exchange (Ruckdeschel et al., 2017). Owing to the low thermal conductivity of HGM, the heat conduction path in composites is longer, the thermal resistance is greater, and the temperature preserved performance is better. Therefore, heat transport in HGM-EP composites includes three main methods (Chau et al., 2017; Xing et al., 2020): (1) gaseous convection within the HGM; (2) thermal radiation on the surface of the HGM; and (3) solid and gaseous conduction. After different hydrostatic pressure treatments, some of the HGM is broken (as shown in Fig. 9). It can also be seen in Fig. 11, after treatment at a high hydrostatic pressure of 60 MPa, obvious cracks are formed on the wall of HGM, and lots of fragments appear, which are significantly different from composites without high hydrostatic pressure treatment. Finally, the water absorption rose sharply. Then, pressurized water filled the space of the broken HGM; thereby two new heat transfer methods are added (as shown in Fig. 12): heat conduction and convection of liquid. Compared with the thin gas inside the HGM, the heat conduction and convection of the liquid is significantly greater than that of the gas, which causes the temperature preserved performance of the composites to decrease. And the pores filled with water is also the reason why the thermal

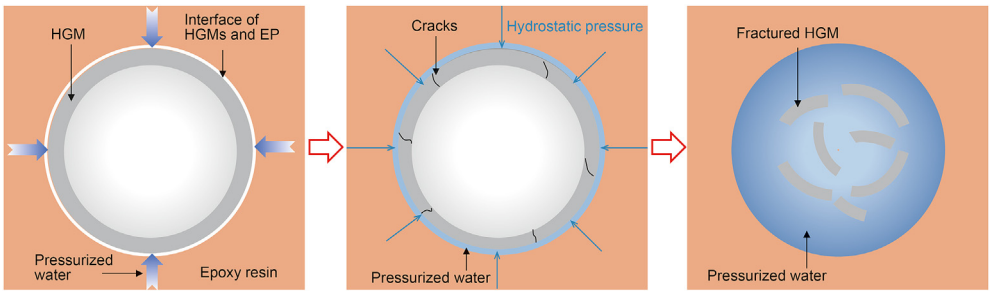

Fig. 9. A schematic of high-pressure water invading the composites.

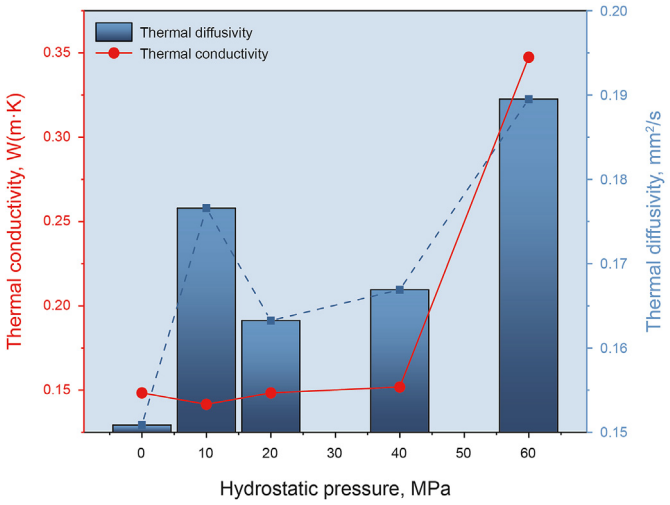

Fig. 10. Thermal conductivity and thermal diffusivity of composites after different hydrostatic pressure treatments.

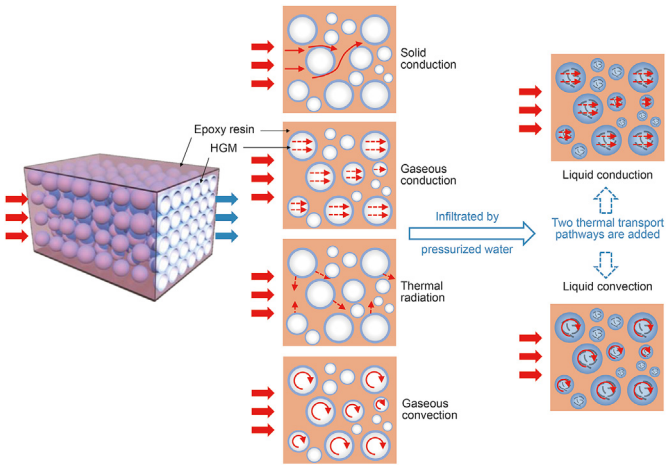

Fig. 12. A schematic of thermal transport pathways in HGM/EP composites.

conductivity of the composites increases sharply after being treated by 60 MPa hydrostatic pressure in Fig. 10. Improving the strength of the microspheres or interface might improve this defect, which is the next stage of research. The same is true for any insulation material. In the application of temperature-preserved materials, it is necessary to avoid the enhancement of heat conduction and convection caused by water entering the pore structure of materials. And the superimposed high-temperature environment will aggravate the heat transfer process. Therefore, it is very important to avoid high hydrostatic pressure water invading materials in the ITP-coring process.

In conclusion, from the perspective of temperature preserved performance, composites with 50 vol% HGM are only suitable for ITP-Coring in a hydrostatic pressure environment lower than 40 MPa.

3.3. The change of mechanical properties of composites after hydrostatic pressure treatment

Composites still need to meet the strength and strain capacity required for deep coring operations under hydrostatic pressure. As shown in Fig. 13 (a), the change of compressive strength and strain is consistent with water absorption and thermal conductivity. When the hydrostatic pressure reaches 60 MPa, the compressive strength of the composites significantly decreases by about 41.09%, while the compressive strain increases by about 44.03%. As shown in Fig. 13 (b), the tensile strength presents a small fluctuation due to the large dispersion, but the tensile strain also increases by about 41.11%. When the hydrostatic pressure is 40 MPa, the tensile strain of the composites is 1.08%, which meets the design requirements of the temperature preserved corer and is consistent with the aforementioned conclusion.

Water molecules will invade the macromolecular segments of the resin matrix under pressure, resulting in a decrease in strength. Meanwhile, water can combine with the polar groups of the matrix and has a plasticizing effect on the matrix, which causes the strain of the material to increase. The compressive elastic modulus of the composites is also greatly reduced after 60 MPa hydrostatic pressure treatment (as shown in Fig. 14). This is because the water pressure causes most HGM with high brittleness to break or deboned from the matrix.

In order to further explain the mechanism of the change of composite strains after different hydrostatic pressure treatments, the stress-strain curve is analyzed. As shown in Fig. 15, the compressive stress-strain curves of composites show three obvious stages: elastic region, yield region, and plateau region. The stress-strain curve has obvious differences as the pressure reaches 60 MPa, which is mainly reflected in the longer platform stage. And it is also the main reason for the increase in compressive strain. The plasticizing effect of water on the matrix, resulting in the matrix framework around pores, HGM and crushed HGM, can no longer support the external load, causing this part of the space to be further compressed. Finally, the larger compressive strain is formed.

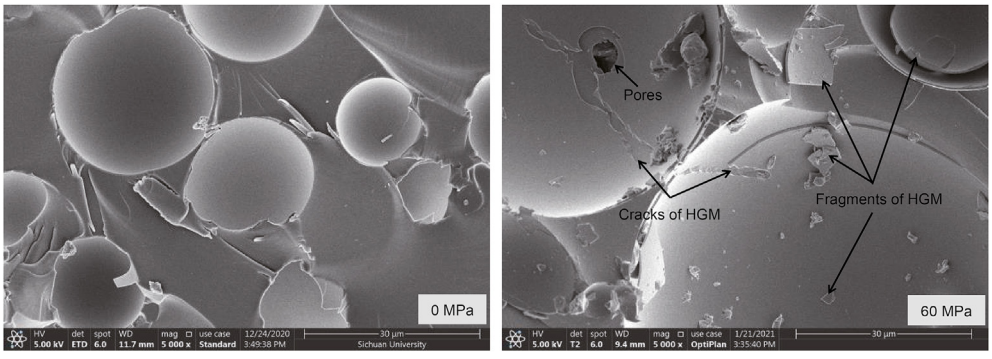

Fig. 11. SEM images of high-pressure water invading the composites.

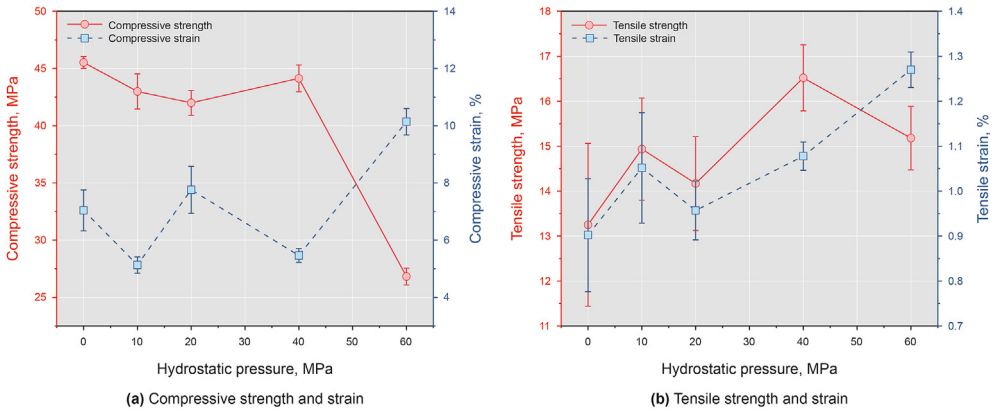

Fig. 13. The change of strength and strain of composites after different hydrostatic pressure treatments.

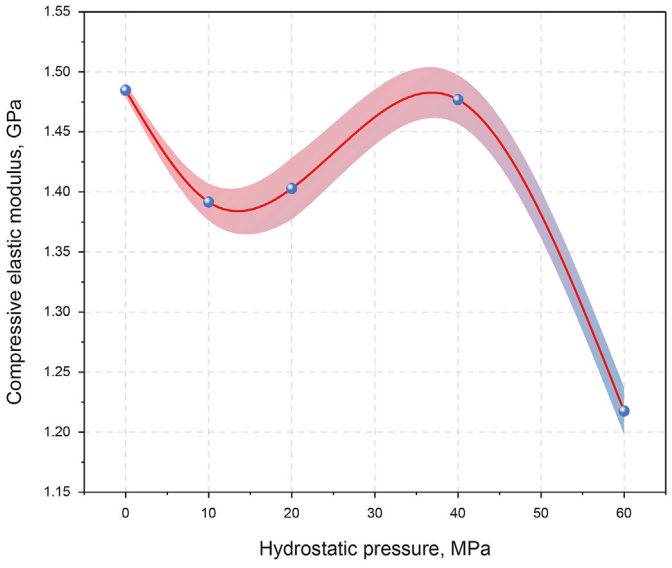

Fig. 14. The change of compressive elastic modulus of composites after different hydrostatic pressure treatments.

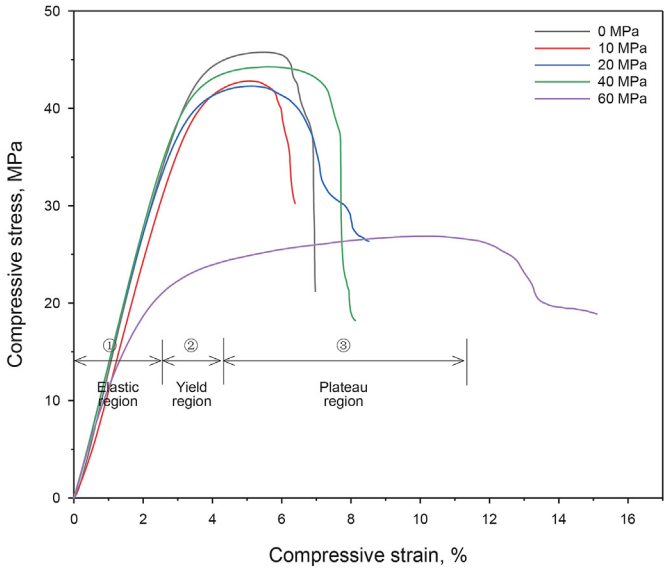

Fig. 15. The compressive stress-strain curves of composites after different hydrostatic pressure treatments.

4. Composite temperature preserved performance and heat transfer model

4.1. Temperature preserved test and heat transfer model

Based on the aforementioned test results, we believe that the composites with 50 vol% HGM is suitable for ITP-Coring in 40 MPa hydrostatic pressure environment. Finally, the temperature preserved performance of composites in engineering applications was studied. Composites are arranged in a two-layer pipe in a sandwich structure, with a thickness of 6 mm, as shown in Fig. 16. The successful injection and curing of the composites prove the feasibility of this scheme. In the beginning, hot water at about 80 °C is poured into the inner pipe. And three temperature sensors are installed in the lower, middle, and upper of the inner pipe.

As shown in Fig. 17, due to the cover has not been closed, the water temperature drops sharply at the initial stage. Subsequently, the temperature difference between the water temperature in the pipe and the ambient temperature gradually narrowed, so the temperature change shows obvious segmentation. The three curves basically coincide, so the internal water temperature can be considered very uniform.

In order to investigate the temperature preserved mechanism of composites, a heat transfer model was established. Based on the theory of unsteady-state heat transfer, the model is appropriately simplified for the test process, as shown in Fig. 18.

As shown in Fig. 18, according to the single-layer cylindrical heat transfer model, thermal resistance R_1 of the cross-section *A-A* can be obtained by considering the thermal convection and conduction of the radial multilayer cylindrical wall (Yang and Tao, 2006), as shown in Eq. (1):

$$R_1 = \frac{1}{2\pi r_{i1} l h_f} + \frac{\ln(r_{i2}/r_{i1})}{2\pi l \lambda_g} + \frac{\ln(r_{o1}/r_{i2})}{2\pi l \lambda_c} + \frac{\ln(r_{o2}/r_{o1})}{2\pi l \lambda_g} + \frac{1}{2\pi r_{o2} l h_a} \quad (1)$$

where r_{i1}, r_{i2}, r_{o1}, r_{o2} are the inner and outer diameters of the inner pipe, and the inner and outer diameters of the outer pipe, respectively, which are 0.03, 0.033, 0.039, 0.049 m, respectively; l is the height of the model, which is 0.26 m; λ_g is the thermal conductivity of the metal, which is 16.27 W/(m·K); λ_c is the thermal conductivity of the composites, and according to the test results, 0.15 W/(m·K) can be obtained; h_f is the convective heat transfer coefficient of the internal fluid and the pipe, which is 150 W/(m^2·K); and h_a is the

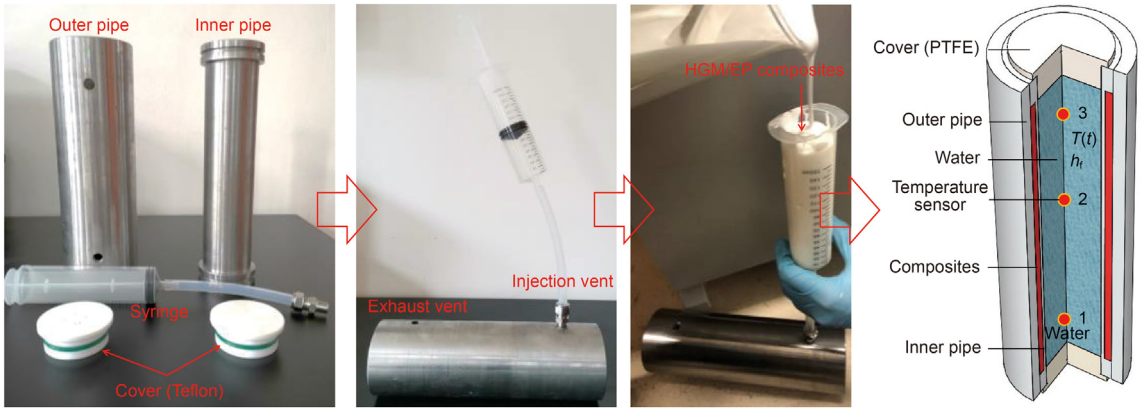

Fig. 16. Temperature preserved performance test of composites.

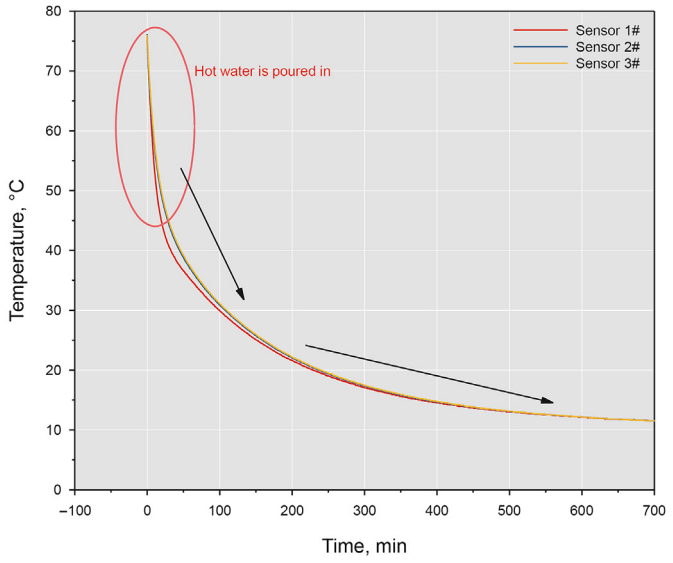

Fig. 17. Temperature preserved performance of composites.

convective heat transfer coefficient of the pipe and ambient, which is 10 W/(m^2·K).

Because the height to diameter ratio of the model is relatively small, the cover needs to be considered into the calculation. The thermal resistance of the upper and lower covers is R_2, R_3, as shown in Eq. (2):

$$R_2 = R_3 = \frac{1}{h_f \pi r_{i1}^2} + \frac{\delta}{\lambda_g \pi r_{i1}^2} + \frac{1}{h_a \pi r_{i1}^2} \tag{2}$$

where δ is the thickness of the PTFE cover, which is 0.025 m.

Therefore, the total thermal resistance of the model can be calculated by Eq. (3).

$$R = 1/(1/R_1 + 1/R_2 + 1/R_3) \tag{3}$$

Since the internal water temperature is uniform, assuming that the water temperature at any time is $T(t)$, Eq. (4) can be obtained according to the conservation of energy:

$$m_w c_w (T_0 - T(t)) = \int \frac{T(t) - T_a}{R} dt \tag{4}$$

where m_w is the mass of water, kg; c_w is the specific heat capacity, J/(kg·°C); $T(t)$, T_0 are the temperature at any time and initial temperature of the water, respectively, °C; T_a is the ambient temperature, °C; R is the total thermal resistance, °C/W; t is the time, min.

According to the initial conditions, the water temperature at any time can be obtained, as shown in Eq. (5):

$$T(t) = e^{\left[-\frac{1}{m_w c_w R} t + \ln(T_0 - T_a)\right]} + T_a \tag{5}$$

Take the water temperature collected by sensor 2 as an example, and the established heat transfer model is compared with test results, as shown in Fig. 19. In the initial cooling stage, due to the hot water just pouring in, the curve shows a sharp drop, which leads to a large gap to the theoretical results. As the heat dissipation process continues, the theoretical and experimental results gradually become consistent, indicating that the heat transfer model has a certain feasibility and credibility in predicting actual temperature change.

Fig. 20 shows the theoretical results of the temperature preserved performance of different composites. The increase in the HGM content leads to a decrease in the thermal conductivity of the composites, thereby reducing the heat exchange rate between the water in the pipe and the ambient, and improving the temperature preserved performance. However, due to the increased in thermal conductivity of the composites after 60 MPa hydrostatic pressure treatment, the cooling rate is even higher than that of the composites with 0 vol% HGM.

4.2. Heat transfer model in coring process based on HGM/EP composites

After the coring process, the ambient temperature is constantly changing during core lifted. Therefore, the method of considering the ambient temperature as a constant in the heat transfer model will no longer be suitable. Meanwhile, the actual corer size and the design of the temperature preserved scheme must also be considered. The schematic of the core chamber is shown in Fig. 21, where the core diameter is 50 mm, the thickness of the composite is 10 mm, and the water and marble are considered as the media in the chamber.

Assuming the core lifting speed is v, and the geothermal gradient is ΔT per 100 m. And the ambient temperature around the chamber is consistent with the formation temperature, then the change of the ambient temperature T_a during the core lifting in time t is shown in Eq. (6):

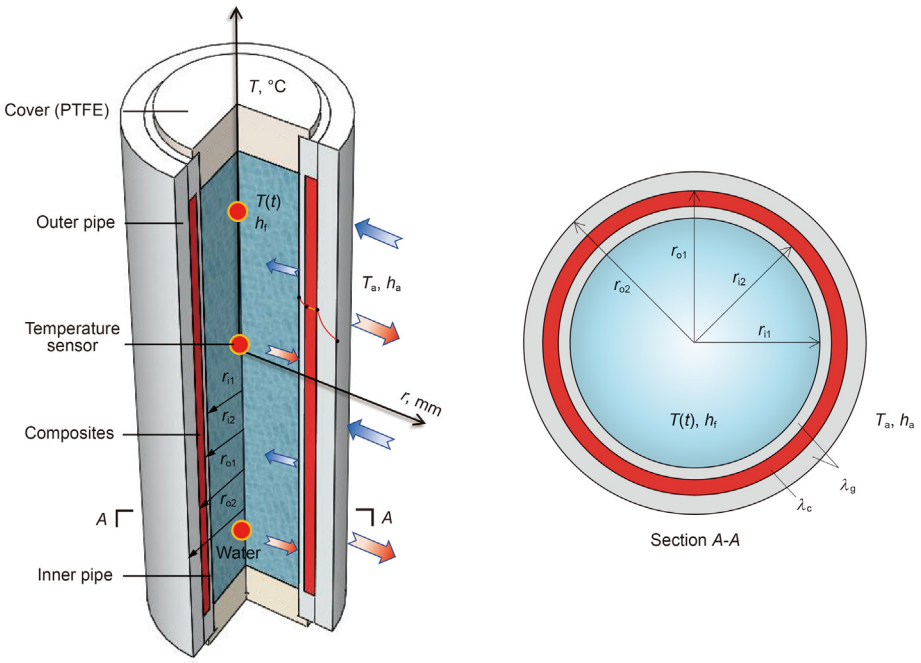

Fig. 18. Simplified heat transfer model.

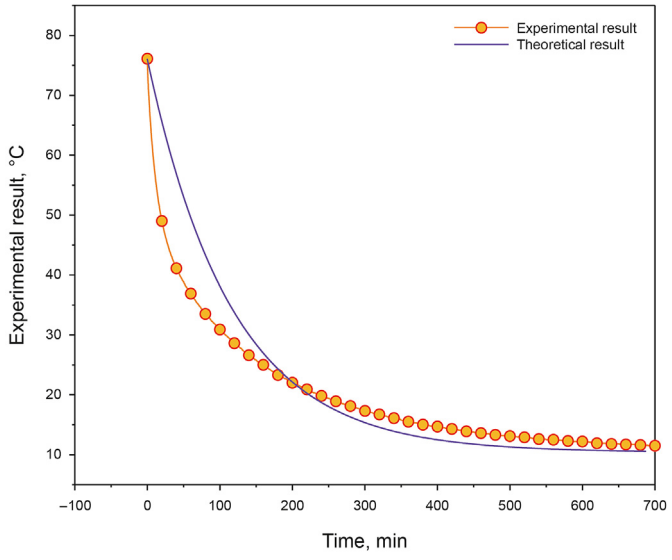

Fig. 19. Comparison of the theoretical and experimental results.

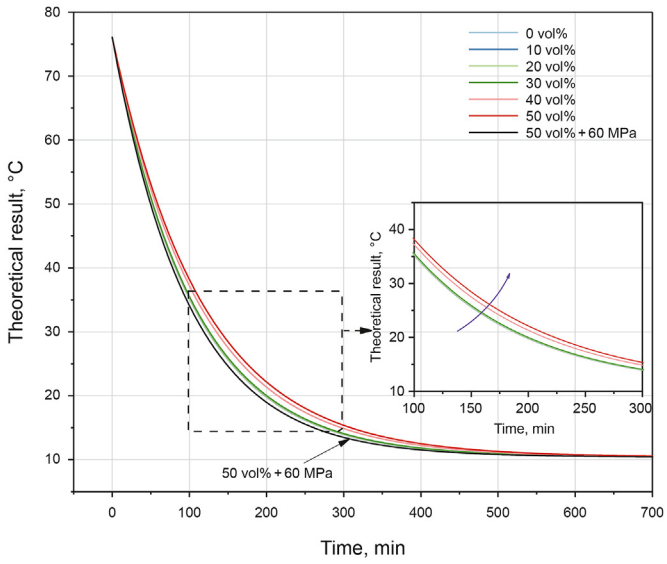

Fig. 20. The theoretical results of the temperature preserved performance of different composites.

$$T_a = T(0) - (v^*t/100)^*\Delta T \tag{6}$$

where $T(0)$ is the ambient temperature, °C; v is the lifting speed, m/s; ΔT is the geothermal gradient, °C/100 m.

Therefore, the temperature of the media inside the chamber $T(t)$ during the lifting process can be calculated by substituting the chamber size and Eq. (6) into Eq. (4). Then, $T(t)$ and T_a are both functions of time t.

$$(m_w c_w + m_M c_M)(T_0 - T(t)) = \int \frac{T(t) - T(0) + (vt/100)\Delta T}{R_C} dt \tag{7}$$

where m_M is the mass of the marble, kg; c_M is the specific heat capacity of the marble, J/(kg·°C); R_C is the total thermal resistance of the core cabin, °C/W.

Considering $t = 0$, the initial temperature $T(t) = T(0)$, and the cooling rate $T'(t) = T'(0) = 0$. Therefore, the internal media temperature change at any time during the core lifting process is obtained, as shown in Eq. (8):

$$T(t) = \frac{v\Delta T}{100}\left[(m_w c_w + m_M c_M)R_C\left(1 - e^{-\frac{t}{(m_w c_w + m_M c_M)R_C}}\right) - t\right] + T(0) \tag{8}$$

The total thermal resistance R_C of the core chamber can be

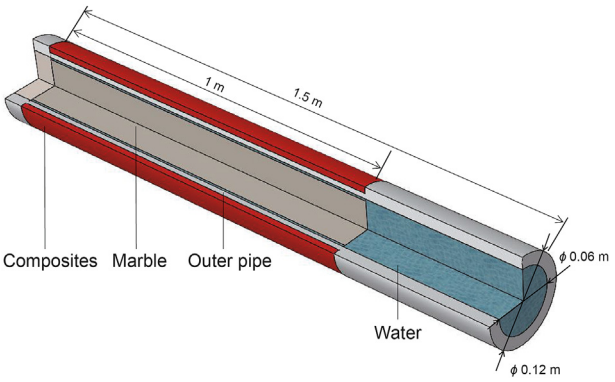

Fig. 21. The schematic of the core chamber of the corer.

calculated according to the actual size in Fig. 21. Due to the long size of the chamber, the heat dissipation is mainly caused by the radial cylindrical wall, so the thermal resistance at both ends is ignored here. R_C is shown in Eq. (9).

$$R_C = \frac{1}{\frac{1}{\frac{1}{2\pi r_{g1} l_c h_f} + \frac{\ln\left(r_{g2}/r_{g1}\right)}{2\pi l_c \lambda_g} + \frac{\ln\left(r_c/r_{g2}\right)}{2\pi l_c \lambda_c}} + \frac{1}{\frac{1}{2\pi r_{g1} l_g h_f} + \frac{\ln\left(r_c/r_{g1}\right)}{2\pi l_g \lambda_g}}} + \frac{1}{2\pi r_{g2} l_t h_a} \tag{9}$$

where r_{g1}, r_{g2}, r_c are the inner and outer diameters of the outer pipe at the groove and the outer diameter of the composites, m; l_t is the total length of the core chamber, m; l_c is the length of the composites, m; l_g is the length of the outer pipe at the lower end of the composites, m.

After obtaining the change of the core temperature, the heat loss and heat dissipation power during this process can be simply evaluated by Eq. (10).

$$Q = (m_w c_w + m_M c_M)\Delta T(t) = Pt \tag{10}$$

where $\Delta T(t)$ is the temperature change during core lifting, °C; Q is the heat loss, J; P is the heat dissipation power, W.

Considering that the normal temperature is 25 °C, the lifting speed v is 150 m/min, the geothermal gradient ΔT is 4 °C/100 m, and the temperature of the coring formation is 150 °C. Therefore, the theoretical change of the core temperature during the lifting process can be obtained, as shown in Fig. 22. It is observed that the total time of core lifting is about 20.8 min. During the core lifting process, the ambient temperature presents an ideal linear change trend, while the core temperature presents a nonlinear change. Meanwhile, the composites have obvious temperature preserved performance. With and without composites, the core temperature will drop by 21.4 and 24.4 °C, respectively. According to Eq. (10), it can be concluded that the heat loss and heat dissipation power of the core chamber with composites are 291.1 kJ and 232.9 W, respectively. And the heat loss and heat dissipation power of the core chamber without composites are 291.1 kJ and 232.9 W, respectively. In summary, the composites can increase the temperature preserved performance by about 12.2% in the ITP-Coring process. The established model can also provide guidance for engineering applications from a theoretical perspective. Meanwhile, we have put forward the concept of the active temperature preserved coring method and carried out related researches (Xie et al., 2020). Then, the composites will help realize the active temperature preserved scheme under the conditions of effective space and energy supply.

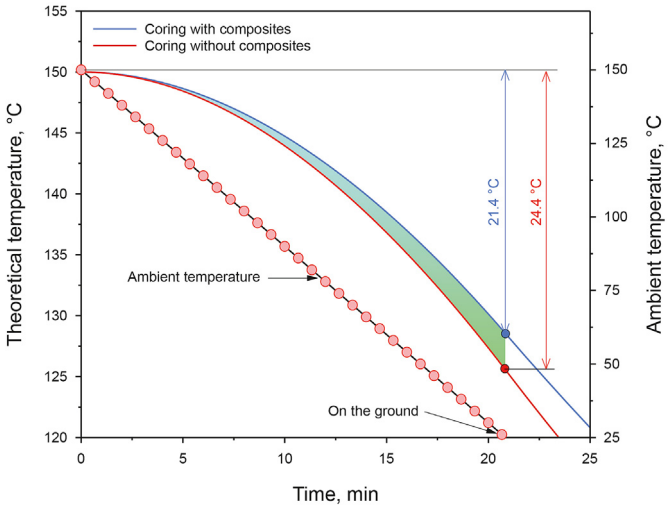

Fig. 22. The theoretical change of the core temperature during lifting process.

5. Conclusions

Focusing on deep rock ITP-Coring technology, it is innovatively proposed to use HGM/EP composites as temperature preserved materials. The physical, mechanical and temperature preserved properties of the composites were evaluated, and a heat transfer model in the coring process based on HGM/EP composites was established, which could provide guidance for engineering applications from a theoretical perspective. The following conclusions were drawn:

(1) When the hydrostatic pressure reaches 60 MPa, the water absorption of composites with 50 vol% HGM increases to more than 30.19%, and the thermal conductivity increases by about 2.34 times.
(2) Above 40 MPa, the water can weaken the mechanical properties of composites. On the contrary, the performance of the composites are almost unaffected. Therefore, composites with 50 vol% HGM are suitable for ITP-Coring in a hydrostatic pressure environment of lower than 40 MPa.
(3) The composites are feasible for engineering application. At the same time, the established heat transfer model is consistent with the experimental results and has certain feasibility and credibility.
(4) A heat transfer model in the coring process based on HGM/EP composites with 50 vol% HGM is established. Theoretically, the application of composites may increase the temperature preserved ability by about 12.2%.

Availability of data and material

The raw/processed data required to reproduce these findings cannot be shared at this time as the data also forms part of an ongoing study.

Declaration of competing interest

The authors declare that they have no conflict of interest.

Acknowledgments

The authors gratefully acknowledge the National Natural Science Foundation of China (grant number 51827901). This project

was also funded by the Program for Guangdong Introducing Innovative and Enterpreneurial Teams (No. 2019ZT08G315) and Shenzhen Basic Research Program (General Program) (No. JCYJ20190808153416970).

References

Abegg, F., Hohnberg, H.J., Pape, T., et al., 2008. Development and application of pressure-core-sampling systems for the investigation of gas- and gas-hydrate-bearing sediments. Deep Sea Res. Oceanogr. Res. Pap. 55 (11), 1590–1599. https://doi.org/10.1016/j.dsr.2008.06.006.

Chau, M., Kopera, B.A.F., Machado, V.R., et al., 2017. Reversible transition between isotropic and anisotropic thermal transport in elastic polyurethane foams. Materials Horizons 4 (2), 236–241. https://doi.org/10.1039/c6mh00495d.

Gall, M.L., Choqueuse, D., Gac, P.Y.L., et al., 2014. Novel mechanical characterization method for deep sea buoyancy material under hydrostatic pressure. Polym. Test. 39, 36–44. https://doi.org/10.1016/j.polymertesting.2014.07.009.

Gao, M.Z., Chen, L., Fan, D., et al., 2021a. Principle and technology of coring with in-situ pressure and gas maintaining in deep coal mine. J. China Coal Soc. 46 (3), 885–897. https://doi.org/10.13225/j.cnki.jccs.YT21.0297.

Gao, M.Z., Liu, J.J., Lin, W.M., et al., 2020a. Study on in-situ stress evolution law of ultra-thick coal seam in advance mining. Coal Sci. Technol. 48 (2), 28–35.

Gao, M.Z., Xie, J., Gao, Y.N., et al., 2021b. Mechanical behavior of coal under different mining rates: a case study from laboratory experiments to field testing. Int. J. Min. Sci. Technol. 31 (5), 825–841. https://doi.org/10.1016/j.ijmst.2021.06.007.

Gao, M.Z., Xie, J., Guo, J., 2021c. Fractal evolution and connectivity characteristics of mining-induced crack networks in coal masses at different depths. Geomech. Geophys. Geo-energy Geo-resour. 7 (1). https://doi.org/10.1007/s40948-020-00207-4.

Gao, M.Z., Zhang, J.G., Li, S.W., et al., 2020b. Calculating changes in fractal dimension of surface cracks to quantify how the dynamic loading rate affects rock failure in deep mining. J. Cent. S. Univ. 27 (10), 3013–3024. https://doi.org/10.1007/s11771-020-4525-5.

Gao, M.Z., Zhang, Z., Yin, X.G., et al., 2018. The location optimum and permeability-enhancing effect of a low-level shield rock roadway. Rock Mech. Rock Eng. 51 (9), 2935–2948. https://doi.org/10.1007/s00603-018-1461-x.

Gupta, N., Kishore, Woldesenbet E., et al., 2001. Studies on compressive failure features in syntactic foam material. J. Mater. Sci. 36 (18), 4485–4491. https://doi.org/10.1023/A:1017986820603.

Gupta, N., Zeltmann, S.E., Shunmugasamy, V.C., et al., 2014. Applications of polymer matrix syntactic foams. JOM 66 (2), 245–254. https://doi.org/10.1007/s11837-013-0796-8.

He, Z.Q., Xie, H.P., Gao, M.Z., et al., 2020. Design and verification of a deep rock corer with retaining the in situ temperature. Adv. Civ. Eng. 2020 (11), 1–13. https://doi.org/10.1155/2020/8894286.

Kim, H.S., Plubrai, P., 2004. Manufacturing and failure mechanisms of syntactic foam under compression. Compos. Appl. Sci. Manuf. 35 (9), 1009–1015. https://doi.org/10.1016/j.compositesa.2004.03.013.

Li, S.L., Cheng, Y., Qin, H.W., et al., 2006. Development of pressure piston corer for exploring natural gas hydrates. J. Zhejiang Univ. 40 (5). https://doi.org/10.3785/j.issn.1008-973X.2006.05.033.

Liang, B., Gao, H.M., Lan, Y.W., 2005. Theoretical analysis and experimental study on relation between rock permeability and temperature. Chin. J. Rock Mech. Eng. 24 (12), 2009–2012. https://doi.org/10.3321/j.issn:1000-6915.2005.12.002 (in Chinese).

Norihito, I., Koji, Y., 2015. Data report: hybrid Pressure Coring System tool review and summary of recovery result from gas-hydrate related coring in the Nankai Project. Mar. Petrol. Geol. 66, 323–345. https://doi.org/10.1016/j.marpetgeo.2015.02.023.

Ozturk, U.E., Anlas, G., 2011. Hydrostatic compression of anisotropic low density polymeric foams under multiple loadings and unloadings. Polym. Test. 30 (7), 737–742. https://doi.org/10.1016/j.polymertesting.2011.06.002.

Pang, X.Q., Jia, C.Z., Wang, W.Y., 2015. Petroleum geology features and research developments of hydrocarbon accumulation in deep petroliferous basins. Petrol. Sci. 12 (1), 1–53. https://doi.org/10.1007/s12182-015-0014-0.

Qin, H.W., Gu, L.Y., Li, S.L., et al., 2005. Pressure tight piston corer –A new approach on gas hydrate investigation. China Ocean Eng. 19 (1), 121–128. https://doi.org/10.3321/j.issn:0890-5487.2005.01.011.

Rabbani, A., Baychev, T.G., Ayatollahi, S., et al., 2017. Evolution of pore-scale morphology of oil shale during pyrolysis: a quantitative analysis. Transport Porous Media 119 (4), 1–20. https://doi.org/10.1007/s11242-017-0877-1.

Rothwell, R.G., Rack, F.R., 2006. New techniques in sediment core analysis: an introduction. Geological Society London Special Publications 267 (1), 1–29. https://doi.org/10.1144/GSL.SP.2006.267.01.01.

Ruckdeschel, P., Philipp, A., Retsch, M., 2017. Understanding thermal insulation in porous, particulate materials. Adv. Funct. Mater. 27 (38). https://doi.org/10.1002/adfm.201702256.

Saif, T., Lin, Q., Bijeljic, B., et al., 2017. Microstructural imaging and characterization of oil shale before and after pyrolysis. Fuel 197, 562–574. https://doi.org/10.1016/j.fuel.2017.02.030.

Takahashi, H., Tsuji, Y., 2005. Multi-well Exploration Program in 2004 for Natural Hydrate in the Nankai-Trough Offshore Japan. Offshore Technology Conference, Houston, Texas. http://doi.org/10.4043/17162-MS.

Wang, X.D., 2017. Preparation and Thermal Insulation Mechanism of Resin-Based Lightweight Insulation Composite Materials.

Xie, H.P., 2017. Research framework and anticipated results of deep rock mechanics and mining theory. Advanced Engineering Sciences 49 (2), 1–16. https://doi.org/10.15961/j.jsuese.201700025 (in Chinese).

Xie, H.P., Gao, F., Ju, Y., 2015. Research and development of rock mechanics in deep ground engineering. Chin. J. Rock Mech. Eng. 34 (11), 2161–2178. https://doi.org/10.13722/j.cnki.jrme.2015.1369 (in Chinese).

Xie, H.P., Gao, M.Z., Zhang, R., et al., 2020. Study on concept and progress of in situ fidelity coring of deep rocks. Chin. J. Rock Mech. Eng. 39 (5), 865–876. https://doi.org/10.13722/j.cnki.jrme.2020.0138 (in Chinese).

Xie, H.P., Liu, T., Gao, M.Z., et al., 2021. Research on in-situ condition preserved coring and testing systems. Petrol. Sci. https://doi.org/10.1016/j.petsci.2021.11.003.

Xing, Z.P., Ke, H.J., Wang, X.D., et al., 2020. Investigation of the thermal conductivity of resin-based lightweight composites filled with hollow glass microspheres. Polymers 12 (3). https://doi.org/10.3390/polym12030518.

Yang, S.M., Tao, W.Q., 2006. Heat Transfer, 4 ed. Higher Education Press, Beijing, China.

Yung, K., Zhu, B., Yue, T., et al., 2009. Preparation and properties of hollow glass microsphere-filled epoxy-matrix composites. Compos. Sci. Technol. 69 (2), 260–264. https://doi.org/10.1016/j.compscitech.2008.10.014.

Zhai, G.J., Ding, Y., Wang, Y., et al., 2020. Experimental investigation of the hydrostatic compression of a hollow glass microspheres/epoxy resin under high-pressure conditions at the full ocean depth. Polym. Compos. 41 (12). https://doi.org/10.1002/pc.25797.

Zhang, X.S., Wang, H.J., Ma, F., et al., 2016. Classification and characteristics of tight oil plays. Petrol. Sci. 13 (1), 18–33. https://doi.org/10.1007/s12182-015-0075-0.

Zhao, J., Yang, D., Kang, Z., et al., 2012. A micro-CT study of changes in the internal structure of Daqing and Yan'an oil shales at high temperatures. Oil Shale 29 (4). https://doi.org/10.3176/oil.2012.4.06.

Zhou, X.Y., Pang, X.Q., Li, Q.M., et al., 2010. Advances and problems in hydrocarbon exploration in the Tazhong area. Tarim Basin. Petroleum Science 7 (2), 164–178. https://doi.org/10.1007/s12182-010-0020-1.

Zhu, H.Y., Liu, Q.Y., Deng, J.G., et al., 2013. A pressure and temperature preservation system for gas-hydrate-bearing sediments sampler. Petrol. Sci. Technol. 31 (6), 652–662. https://doi.org/10.1080/10916466.2010.531352.

Zhu, H.Y., Liu, Q.Y., Deng, J.G., et al., 2011. Pressure and temperature preservation techniques for gas-hydrate-bearing sediments sampling. Energy 36 (7), 4542–4551. https://doi.org/10.1016/j.energy.2011.03.053.